Flexural Performance of UHPC Beams with Externally Prestressed Plain CFRP Tendons

Authors: Qizhi Xu, Yuqing Tan, Kaiwei Lu, Wendel Sebastian, Jingquan Wang

### **Abstract**

This paper reports the flexural performance of ultrahigh-performance concrete (UHPC) beams externally prestressed with carbon fiber-reinforced polymer (CFRP) tendons. To consider the influence of concrete strengths, prestressing levels, and external CFRP tendon diameters on their failure modes, crack distribution, load-midspan deflection, stress increment-midspan deflection relationship, and ductility, this study entailed six simply supported beams. The test results show that, as the initial prestressing force increased, the failure modes changed from the peeling off of UHPC to the crushing of UHPC and fracture of the CFRP tendon. Replacing the normal concrete with UHPC improved the ultimate strength by 50% and reduced the maximum crack width from 0.3 to 0.2 mm. Increasing the initial prestress by 21% and 44% in the 8- and 11-mm-diameter CFRP tendons resulted in 14% and 38% higher cracking loads, respectively, with a wider domain of UHPC sharing the loads, which became more pronounced as the diameter of the CFRP tendon increased. The denser and shorter crack distributions were compatible with the structural whole-dependent deformation, resulting in higher structural ductility. The stress increment in the external CFRP tendon increased linearly with the midspan deflection, mainly during the postyielding stage. Finally, the ultimate flexural strength was evaluated and compared with those obtained using current calculation methods.

## Introduction

Over the last few decades, external prestressing technologies have shown promise in accelerating bridge construction and repairing bridge components. Relative to the tendon system where prestressing is performed internally, the thickness of the web of the cross section can be reduced because the tendons and ducts are placed outside the concrete section, leading to a reduction in the structural dead load. Additionally, the external post-tensioning method is regarded as a popular technique in new construction and in strengthening existing structures (Gao et al. 2020),

1

owing to its more economical construction, easier tendon layout placement, and convenient adjustment of the pretension forces in the tendons (<u>Harajli 1993</u>).

However, extending the service life of externally prestressed normal concrete (NC) members in long-span bridges is often challenging due to higher repeated vehicle loads and extreme corrosion conditions. When external prestressing tendons are used, carbon fiber–reinforced polymer (CFRP) tendons instead of steel tendons are advantageous for developing bridges with reduced self-weight and avoiding corrosion-related problems owing to their low weight, high tensile strength, fatigue tolerance, and corrosion resistance under long-term service (Wang et al. 2024).

To date, several studies have been conducted on externally prestressed concrete (EPC) beams with CFRP tendons. Kim and Meier (1991) tested EPC beams with CFRP tendons and found that they failed because of the rupture of the prestressing strands rather than concrete crushing. Mutsuyoshi and Machida (1993) also noticed that EPC beams had a similar load deflection response to those prestressed with steel tendons, and their ductility increased under higher prestressing forces. Kato and Hayashida (1993) reported that EPC beams with hybrid tendons failed in a brittle manner. As revealed by Shahrooz et al. (2002), the external posttensioning CFRP tendons strengthened the degenerate beams owing to their independence from the concrete-CFRP bond quality and improved the stiffness, load-carrying capacity, and ductility of the specimens. Grace et al. (2006) further demonstrated that EPC beams with hybrid (bonded and unbonded) tendons had a higher flexure-bearing capacity than the corresponding bondprestressed specimens, in which the flexural response and failure modes were affected by the initial pretensioning force levels. Elrefai et al. (2008) confirmed that post-tensioning CFRP tendons are efficient in increasing structural stiffness and fatigue life. Lee et al. (2015) proposed a theoretical model to predict the load-deflection relationship of simply supported beams with internal unbonded prestressing CFRP tendons in flexure. Le et al. (2018, 2019) investigated the flexural performance of precast segment concrete beams prestressed with external steel and CFRP tendons. It was found that the beam with internal unbounded CFRP tendons behaved in a manner similar to that with steel tendons; however, ultimately, the rupture of the CFRP tendons caused a sudden load drop compared with the ductile failure of the steel tendon specimen. Similarly, Le et al. (2020) proved that precast segmental concrete beams, prestressed with external steel and CFRP tendons, exhibited adequate load-carrying capacity and ductility after

joint opening. Besides, Sturm et al. (2020) found that the specimens with external CFRP tendon rupturing could carry a 12% higher load at a crack width of 0.3 mm and bore a 35% higher ultimate load than those with external steel tendon fracturing. Gao et al. (2020) experimentally demonstrated that strengthening via external FRP tendons could reduce the tensile stress in both concrete and steel reinforcements but result in a larger ultimate compressive strain. Moreover, Wang et al. (2024) tested prestressed NC beams with internal post-tensioned CFRP strands under flexure and found that NC crushing failure could not fully use the tensile strength of the prestressing strands, leading to reduced ductility.

Except for the corrosion-related issues of external tendons, ultrahigh-performance concrete (UHPC), as opposed to NC, was considered a perfect solution for achieving durability, enabling lightweight and longer-span prestressing concrete bridges because it requires less maintenance for smaller sections, owing to its high compressive (>150 MPa) and tensile (>7 MPa) strengths and superior postcracking behavior (Terrasi 2012). UHPC has been used on a large scale in the Nanjing Fifth Yangtze River Bridge, which is a steel-UHPC composite beam cable-stayed bridge with a main span of 600 m. When UHPC containing coarse aggregate was specially developed and used in the entire bridge deck, the concrete slab thickness could be reduced from 280 to 170 mm, decreasing the consumption of concrete and steel by 40% and 25%, respectively. Thus, the material cost could be compensated by the improved high performance of the structure during its entire service life. A comparative study by Wu et al. (2021) clarified that post-tensioned beams provide 101.45% and 56.47% higher cracking and ultimate moments, respectively, than their non-prestressed counterparts. Logically, an externally prestressed CFRP tendon with a tensile strength of over 2,000 MPa operating with UHPC can mostly exploit both the tensile strength of the CFRP tendon and the compressive strength of UHPC to enhance structural cracking and ultimate loads. More attention should be paid to the anchorage performance at the ends of the prestressing tendons because of the weak strength transversal to the fiber direction in the unidirectional CFRP tendons (Kim and Meier 1991). The UHPC employed with the prestressed CFRP tendons potentially supported a larger global deformation, resulting in a higher compressive force at the anchorage ends, which matched well with the high strength of UHPC. Fang et al. (2020) studied the fatigue behavior of stirrup-free reactive powder concrete beams prestressed with CFRP tendons and proposed the accumulated fatigue damage model. Moreover, Sun et al. (2023) tested the flexural behavior of pretensioned

prestressed NC-UHPC composite beams reinforced with CFRP bars and found that partially replacing the concrete with UHPC in the compressive zone greatly improved the overall flexural deformation. The strain-hardening properties of the UHPC resulted in multiple cracks that fully exploited the strength of the CFRP bars, thereby increasing the ultimate load and displacement.

The ultimate bearing capacity of the externally prestressed concrete beams depends almost entirely on the external tendon stress at failure (Dall'Asta et al. 2007). In contrast to the flexure analysis of internally bonded prestressed members relying on the force equilibrium and strain compatibility across the depth of the critical section, the ultimate stress in the external prestressing members is governed by the global deformation of the entire beam—tendon structural system, in which the second-order effect can be neglected if two deviators were located at the third point of the span (He and Liu 2010). Replacing the steel tendons with CFRP tendons led to another issue in the overall analysis, especially in the approach to failure, which is that the weak transverse shear resistance of the CFRP tendons could inhibit the full longitudinal tensile strength (Ghallab and Beeby 2005). These factors directly affect the failure modes and ultimate stress increments of external tendons.

The literature review revealed that previous studies focused on the flexural performance of prestressed FRP bar–reinforced concrete beams. The flexural behaviors of prestressed CFRP tendons operating with UHPC beams are poorly understood. First, one potential limitation is that conventionally practical tensioning and anchorage systems for engineering applications should be developed and studied, especially for large-scale specimens with high prestress levels in CFRP tendons. Second, few studies have tested the flexural performance of externally prestressed UHPC (EPU) beams with CFRP tendons. From the perspective of the two high-strength materials at the structural level, it is expected that such a system could have a higher load-bearing capacity and better ductility to overcome the brittleness and insufficient ultimate loads controlled by the incompatibility between the brittle NC and linear CFRP tendons. Additionally, whether major factors, such as the prestressing level, CFRP tendon diameter, and concrete strength, produced different structural performances from the EPC beams should be further clarified and validated. Unfortunately, only limited studies are available to understand its flexural behavior; hence, further efforts should be made.

To this end, six specimens, including one EPC and five EPU beams with CFRP tendon members, were tested in flexure to consider the influences of the initial effective prestressing forces, concrete strengths, and CFRP tendon diameters on the failure modes, load–midspan deflection relationships, and stress increments in the external tendons. The tested ultimate stress in the external CFRP tendons and flexural capacities were predicted and compared with those obtained using existing calculation methods. These results provide insights into EPU members with CFRP tendons and contribute to the development of an accurate theoretical model in the future.

## **Experimental Program**

## 1. Materials Properties and Measurements

The UHPC used in this study was commercially produced and mainly consisted of a ready-mix powder, comprising cement, silica fume, ground quartz, and quartz sand. The 0.2-mm-diameter and 13-mm-length straight steel fibers with an ultimate tensile strength of 2,800 MPa, plasticizer, water reducer, and water were mixed proportionally, as listed in Table 1.

**Table 1**. Composition and properties of the UHPC

Property	Value
Weight of components (kg)	13.30
Cement	1,500
Sand	618
Water	173
Water reducer	31
Steel fiber	179
rism compressive strength (MPa)	
Average	119

To obtain the compressive strength and elastic modulus, three nonstandard dimensions of  $70 \times 70 \times 210$  mm prisms were tested using an available compressive testing machine with a 1,000 kN load capacity, while three  $30 \times 30 \times 330$  mm dog-bone samples were prepared for testing the UHPC tensile strength. The compressive strength and elastic modulus were  $119 \pm 3.5$  MPa and  $43 \pm 1.0$  GPa, respectively, while the tensile strength was measured to be  $10 \pm 0.8$  MPa. The code GB/T 31387-2015 (GB 2015) specified that the compressive strength of UHPC material was to be obtained using 100-mm-cubic specimens. As per the standard DB/TJ 08-2401-2022 (UHPC 2022), the compressive strength obtained from the prisms was 0.7 times that of the cubic specimen. Therefore, the cubic compressive strength of UHPC in this study was 170 MPa. The

UHPC was first cast along the beam longitudinal span and then in the beam depth direction. In addition, the average compressive strength of the normal concrete used in this study was tested for  $45 \pm 4.3$  MPa.

The CFRP bars used in this study were plain round bars with diameters of 8 and 11 mm. The measured diameters were consistent with those provided by the manufacturers. The anchorage behavior of the CFRP tendon is a critical factor affecting the flexural performance of EPU beams, and the influence of end slip cannot be ignored. The challenge of anchoring plain round CFRP rebars was overcome using a novel wedge-type anchorage system different from the common wedge-based anchor for steel tendons. Figs. 1(a-1) show the construction details of the anchor system. As shown in Figs. 1(a-c), two slot seams were manufactured along two orthogonal directions. These did not run through the entire height to ensure integrity. For the 8mm-diameter CFRP tendon anchor system, the lengths of the anchor ring and anchor clip were 125 and 160 mm, respectively. The inner and outer diameters were 18 and 28 mm at the top surfaces and 12 and 28 mm at the bottom surfaces, respectively, resulting in a taper angle of 2.2° on the anchor clip. Similarly, the corresponding anchor clip and anchor ring length for the 11mm-diameter CFRP tendon anchor system were 170 and 210 mm, respectively. As shown in Fig. 1(d), the inner and outer diameters of the top and bottom surfaces were 21 and 31 mm and 15 and 28 mm, respectively, with a taper angle of 2.5°. The anchor clip and anchor system are shown in Figs. 1(e and f), respectively. Compared to previous bond-type anchorages for CFRP tendons (Fang et al. 2020; Wang et al. 2024), the proposed wedge-type anchorage system can ensure compatible deformation along the CFRP tendon as a whole and can be reused after separating the anchorage clip from the anchorage ring by unloading the stress in the CFRP tendons.

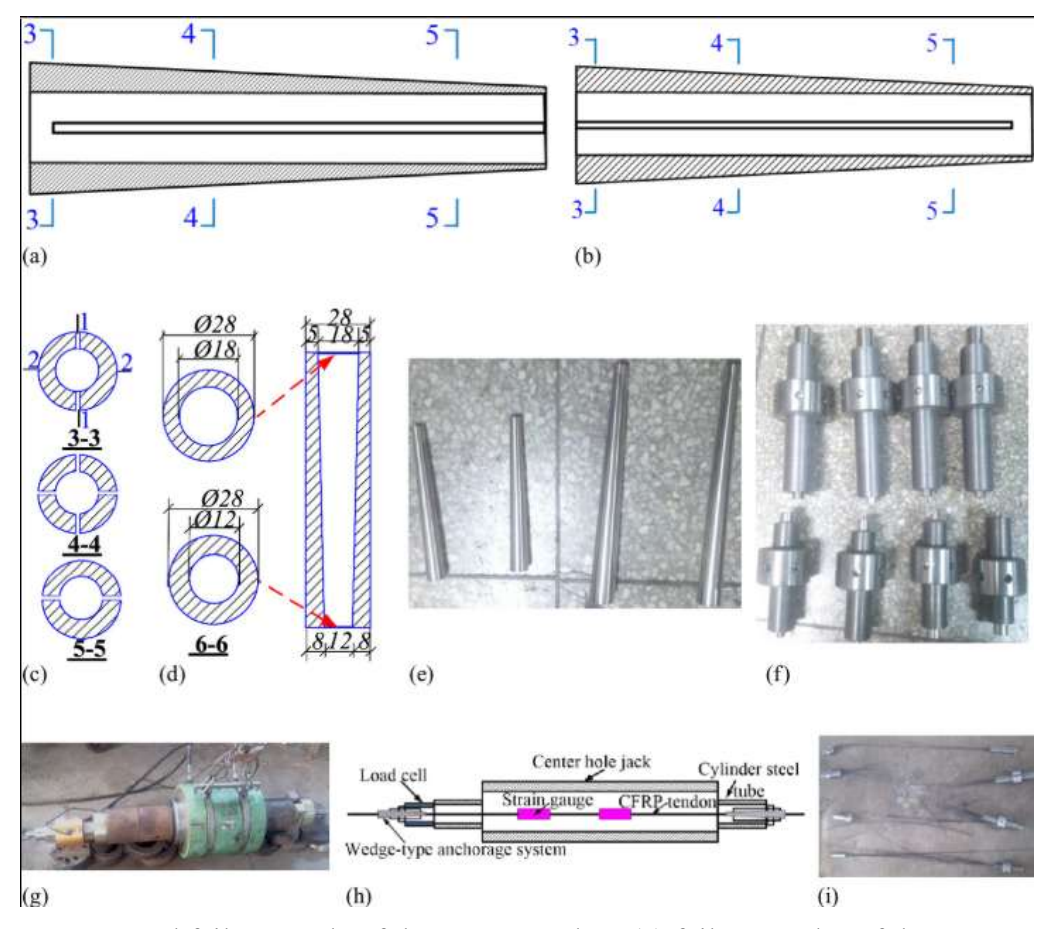


**Fig. 1**. Test setup and failure mode of the CFRP tendon: (a) failure modes of the CFRP tendon; (b) Side view-1 of the anchorage clip; (c) Orthogonal side view-1 of the anchorage clip; (d) bottom view of the anchorage clip; (e) bottom view of the anchorage clip; (f) photographs of the anchorage ring; (g) photographs of the anchorage system; (h) test setup of the CFRP tendon; and (i) schematic of the test setup (dimensions in mm).

Figs.  $\underline{1(g-i)}$  show the test setup for determining the tensile strength of the CFRP tendon anchorage systems. Two strain gauges were attached to measure the tensile strain during the test. The anchorage system behaved well until the CFRP tendons ruptured. The average ultimate tensile strength and elastic modulus of the three 8-mm-diameter CFRP tendons were tested for  $2,057 \pm 99.0$  MPa and  $142.0 \pm 0.5$  GPa, respectively, while these were  $1,925 \pm 56.2$  MPa and  $147 \pm 5.3$  GPa for the 11-mm-diameter CFRP tendons, as summarized in Table  $\underline{2}$ .

**Table 2**. Test results of the material properties of the CFRP tendon

Diameter (mm)	Statistical descriptors	CFI	CF2	CF3	Mean value
8	Ultimate stress (MPa)	1,932	2,174	2,065	2,057
	Elastic modulus (GPa)	142	142	143	142
11	Ultimate stress (MPa)	1,874	1,897	2,003	1,925
	Elastic modulus (GPa)	153	140	147	147

In this study, 16- and 8-mm-diameter steel reinforcements were employed as the longitudinal and transverse reinforcements, respectively. As listed in Table  $\underline{3}$ , their yield and ultimate tensile strengths were tested for  $420 \pm 24$ ,  $576 \pm 16$ ,  $417 \pm 18$ , and  $559 \pm 20$  MPa, respectively.

**Table 3**. Details of the tested specimens

Specimen ID	L (mm)	h × b (mm)	$A_c$ (mm <sup>2</sup> )	f <sub>pe</sub> (MPa)	f <sub>pe</sub> /f <sub>pu</sub>
C-Ø8-0.43	5,200	250 × 120	2Ø8 (100.5)	875	0.43
U-Ø8-0.35	5,200	250 × 120	2Ø8 (100.5)	725	0.35
U-Ø8-0.43	5,200	250 × 120	2Ø8 (100.5)	876	0.43
U-Ø8-0.62	5,200	250 × 120	2Ø8 (100.5)	1,276	0.62
U-Ø <mark>11-0.46</mark>	5,200	250 × 120	2Ø11 (190)	876	0.46
U-Ø11-0.64	5,200	250 × 120	2Ø11 (190)	1,234	0.64

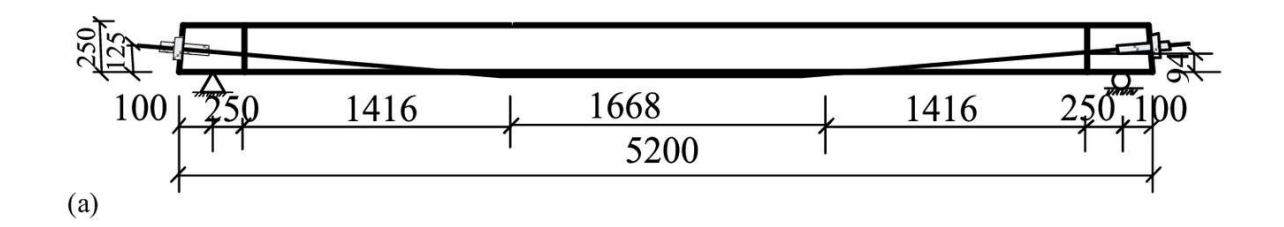
Note: L = specimen span length; h and b = height and width of the cross section, respectively;  $A_c$  = CFRP tendon area; and  $f_{pe}$  and  $f_{pu}$  = effective prestress force and ultimate tensile strength of the CFRP tendon, respectively.

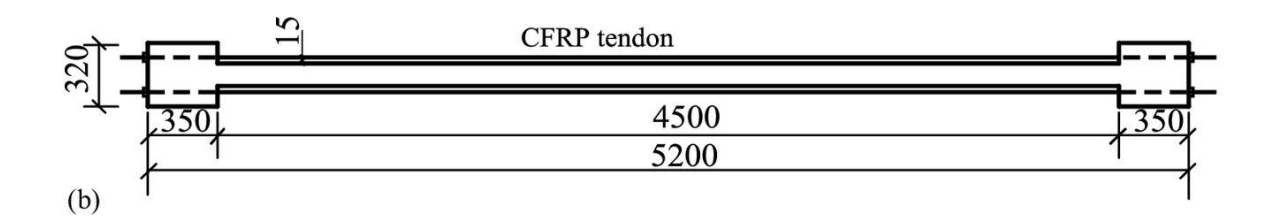
## 2. Specimens Details

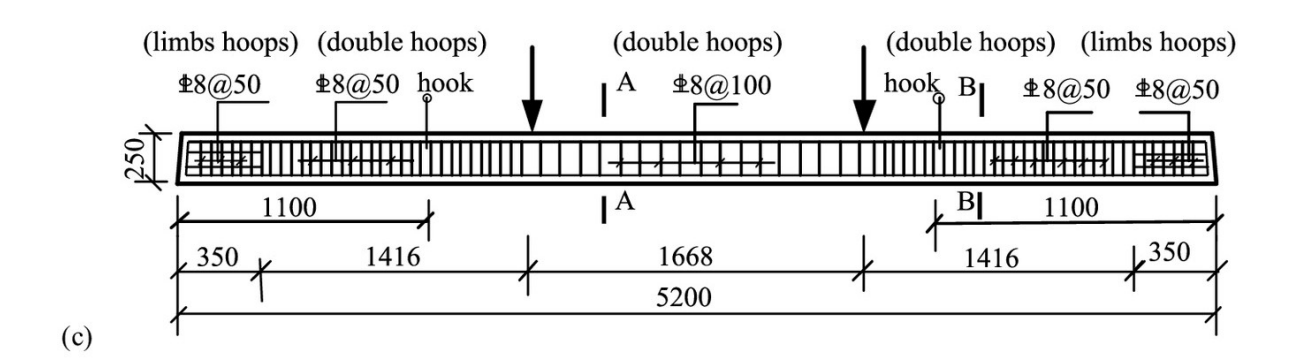
Table 3 lists six tested specimens, including one NC and five UHPC beams, considering the influences of concrete strengths, CFRP tendon diameters, and initial effective prestress levels. Based on Chinese standard JGJ 92-2016 (MOHURD 2016), the pretension stress level was set at  $0.35-0.65f_{pu}$  ( $f_{pu}$  is the ultimate tensile strength of the CFRP tendon). In Table 3, the specimens are labeled on the basis of the concrete type, CFRP tendon diameter, and prestressing force level. For example, Specimens C-Ø8-0.43 and U-Ø11-0.46 refer to the normal concrete

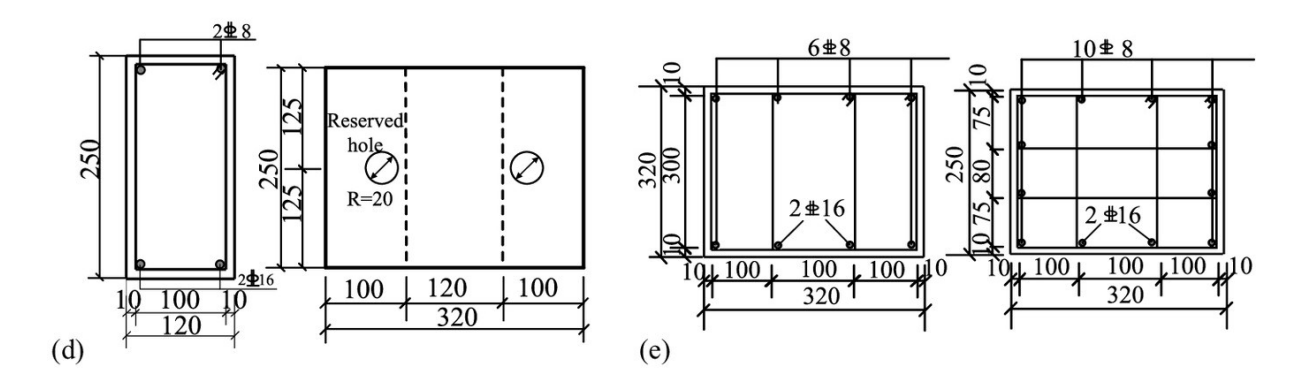
specimen with an 8-mm-diameter CFRP tendon under an initial prestressing stress of  $0.43f_{pu}$  and the UHPC specimen with an 11-mm-diameter CFRP tendon under an initial prestressing stress of  $0.46f_{pu}$ , respectively. Specimen C-Ø8-0.43 was regarded as the benchmark beam.

Figs. 2(a–g) show the details of all six beams with total and clear span lengths of 5,200 and 5,000 mm, respectively, with a 250-mm-height and 120-mm-width rectangular cross section, achieving a clear span-to-height ratio of 20. As shown in Fig. 2(a), four deviators were attached to the two lateral surfaces of the specimen using bolts for the draped tendons to comply with their inclined profiles. Reserve holes were prepared for the screw hole by placing 22-mm-diameter tubes. Similarly, 40-mm-diameter tubes at the end-anchoring part were used to place the CFRP tendon before casting. To effectively anchor the CFRP tendons at the beam ends, larger end sections of 320 mm width, 250 mm height, and 350 mm length reinforced with more steel rebars were constructed to prevent possible concrete splitting failure under high prestressing forces [Fig. 2(b)]. In all beams, two 16-mm-diameter and 8-mm-diameter deformed steel reinforcements served as internal longitudinally bonded non-prestressed bars to support the stirrups, as shown in Figs. 2(c–e). The 8-mm-diameter stirrups were provided at spacings of 50 and 100 mm within the shear span and constant moment regions, respectively.









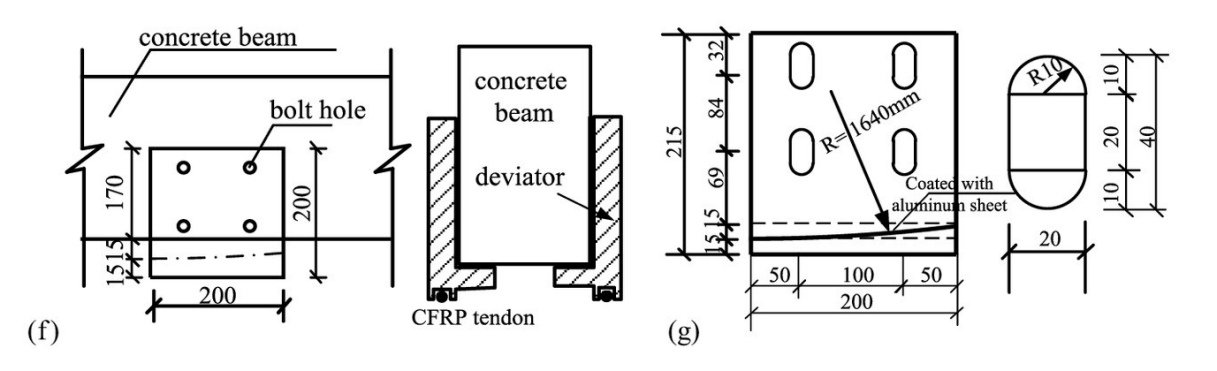


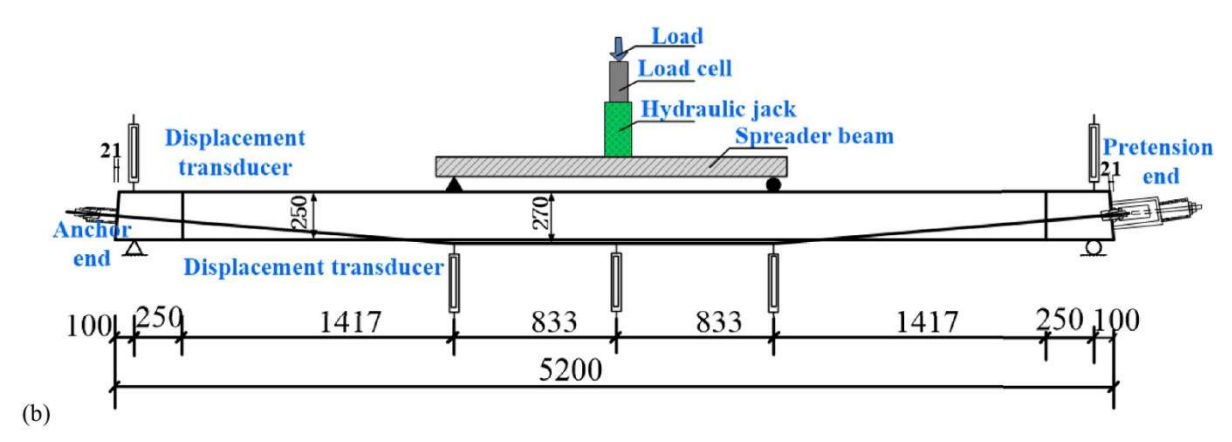
**Fig. 2**. Reinforcement details of the specimen: (a) layout of the externally prestressed CFRP tendon (front view); (b) layout of the external CFRP tendon (elevation view); (c) details of reinforcements (front view); (d) layout of the end anchorage; (e) details of reinforcements at the anchorage end; (f) layout of deviators; and (g) details of deviators (dimensions in mm).

Considering the weaker transverse but stronger longitudinal stiffness of the CFRP tendons, the draped tendon should be carefully considered at the deviator location. The detailed construction design of the deviator is shown in Figs. 2(f and g). A smooth and circular segment instead of a direct point contact was adopted to reduce the stress concentration using an aluminum sheet attached to the inner curved surface within the deviator. Additionally, oil was applied to the aluminum sheet-to-CFRP bar surface to minimize the influence of friction on the ultimate stress of the CFRP tendons.

## 3. Instrumentation and Test Setup

Figs. 3(a and b) show the loading test setup for the specimens. A classic four-point bending test was performed. The distance between the two support ends was 5,000 mm, and the loading points were 1,666 mm apart. As shown in Fig. 3(b), the deflections were measured using five displacement transducers located at the two end supports, two loading points, and midspan. At each loading increment, the cracks were identified and marked, and the maximum crack width at each step was measured and recorded using a microcrack observation instrument. The strain gauges, load cells, and displacement transducer readings were automatically monitored using a computerized data acquisition system (TDS530). Fig. 3(c) presents the strain gauge distributions of the tested beams. Two strain gauges were mounted on the shear spans and constant moment regions to measure the strains of the two CFRP tendons, marked S1–S12, where the numbers in the bracket denote the strain gauges in the opposite CFRP tendon. Additionally, three strain gauges were attached to the internal steel reinforcements within the constant moment region to measure the tensile strain.





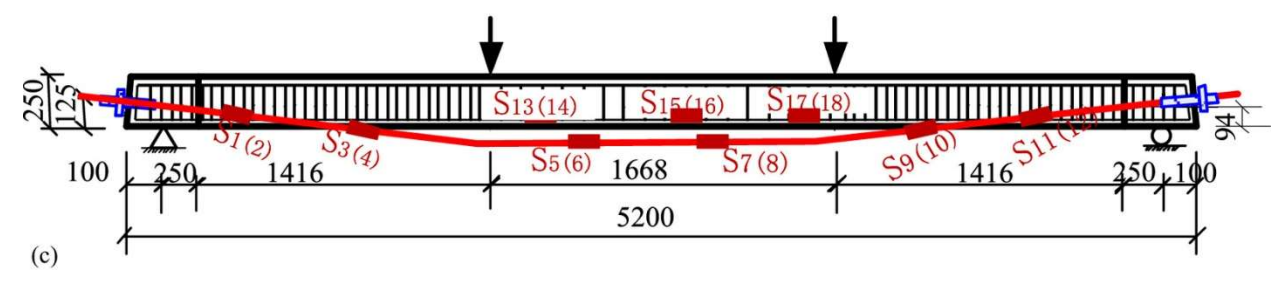


**Fig. 3**. Details of the test setup: (a) test setup; (b) schematic of the setup; and (c) layout of strain gauges (dimensions in mm).

Figs. 4(a—e) show the details and schematic of the deviator, pretension end, and anchorage end in the CFRP tendon. Two CFRP tendons were post-tensioned simultaneously from one end, while the other end was fixed. Attention was paid to balancing the prestressing force in the two CFRP tendons, which were exerted and accurately controlled using the anchor rod pullout instrument HC-20T. Load sensors were installed at the passive anchorages to monitor the effective stress in the tendons, which were also compared with the readings of the strain gauges attached to the

CFRP tendons. Manual operation and continuous adjustment ensured the same target stress levels in the two CFRP tendons.

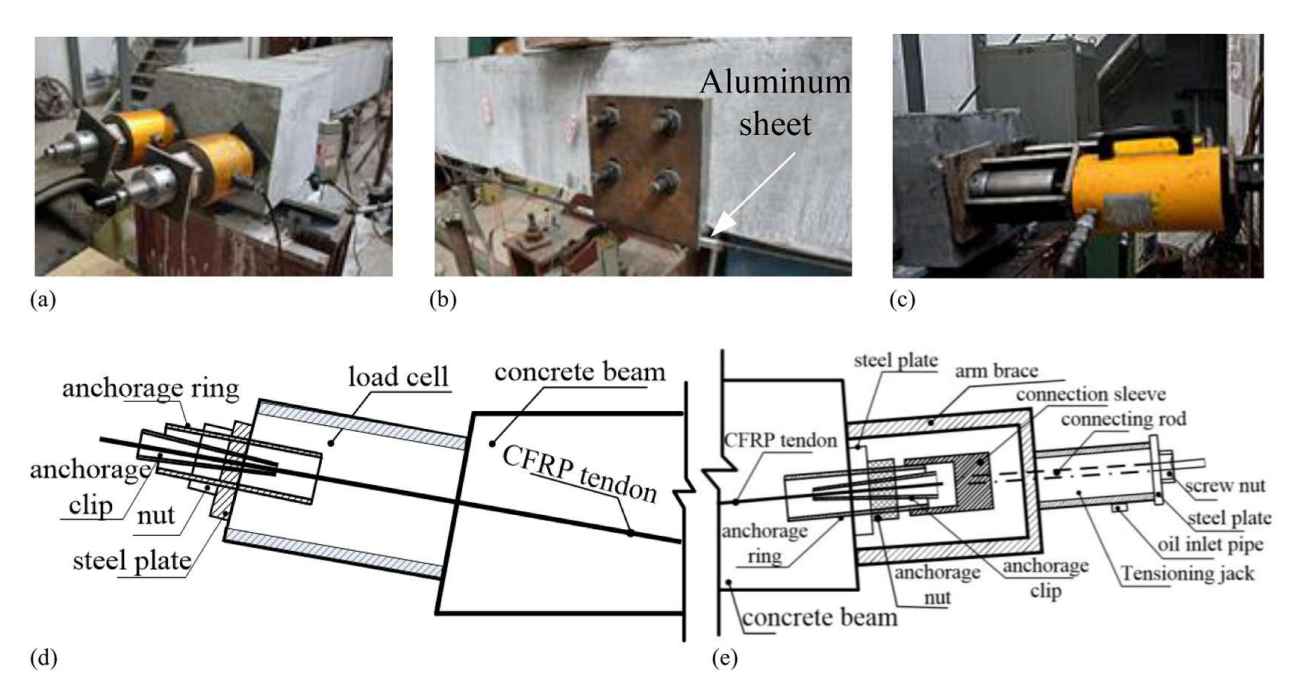


**Fig. 4**. Details of the anchor system of the external CFRP tendons: (a) details of the anchor end; (b) details of the deviator; (c) details of the pretension end; (d) schematic of the anchor end; and (e) schematic of the pretension end.

After reaching the target effective prestress, a force-controlled loading regime was selected via a 1,000-kN-capacity hydraulic jack exerting on the specimen monotonically till failure through a strong distribution beam, which was monitored in real-time using a 100-t-capacity load cell. Trial loading–unloading cycles were conducted before the formal tests to ensure the functionality of the loading system. Subsequently, actual tests were performed with load increments of 5 kN before a visible crack was observed, after which the load increment was increased to 10 kN. Once the internal steel reinforcement yielded, the load increment was decreased to 5 kN until failure occurred. The unloading process was then conducted to obtain the unloading–deflection curves.

### **Test Results and Discussion**

## 4. Characteristics of Failure Modes

All tested beams failed in flexure at either the loading point or midspan. During the test, a mark was placed on the CFRP tendon at the anchoring clip end to observe any possible slip. No visible slip was observed until the CFRP tendon ruptured or the concrete was crushed. Thus, the anchor system was considered to work effectively in maximally exploiting the tensile strength of the CFRP tendon. The external tendon ruptured or split; however, the anchor still held the tendon well was also possible owing to the under-reinforced design. However, the concrete was crushed, and the steel reinforcement yielded at failure, indicating a suitable reinforcement design. If the specimen were over-reinforced, the CFRP tendons would be maintained at a lower stress level and would not fracture until their failure. This study aims to determine the appropriate prestress levels in CFRP tendons to distinguish the crushing of concrete from the tendon rupture. Overall, the proposed anchorage system behaved well until the CFRP tendon fractured, without slipping (Wang et al. 2024).

Typical photos of the failure modes for all the specimens are shown in Fig. 5. Specimen C-Ø8-0.43 failed owing to the concrete crushing. The other five UHPC beams presented three typical failure modes: UHPC or NC crushing without the fracture of CFRP tendons [CC, Fig. 5(a)], the UHPC layer slightly peeling off characterized by slight compressive damage but not as serious as the concrete crushing [UPF, Fig. 5(b)], Specimen U-Ø8-0.62), and UHPC crushing following CFRP tendon fracture [UCF, Fig. 5(c), Specimen U-Ø11-0.64]. In Fig. 5(a), a larger crack width in Specimen U-Ø8-0.43 was observed because the UHPC was crushed at the loading point, resulting in a large beam deflection. As the pretension force level increased, the failure of the UHPC and the large midspan deflection became more pronounced. For the other two failure modes [Figs. 5(b and c)], the CFRP tendons fractured and exploded into many visible single fibers with continuous fracturing sounds. The CFRP tendons in Specimens U-Ø8-0.62 and U-Ø11-0.64 were measured at 0.0139 and 0.0138, respectively, reaching the rupture strain from the material tests, indicating that the high tensile strength of the CFRP tendon was used, thereby validating the effectiveness of the anchorage system. As observed in Fig. 5(c), the CFRP tendons were significantly deflected until their fracture, followed by UHPC crushing, whereas the CFRP tendons fractured before the UHPC peeling off, as observed clearly in Fig. 5(b).

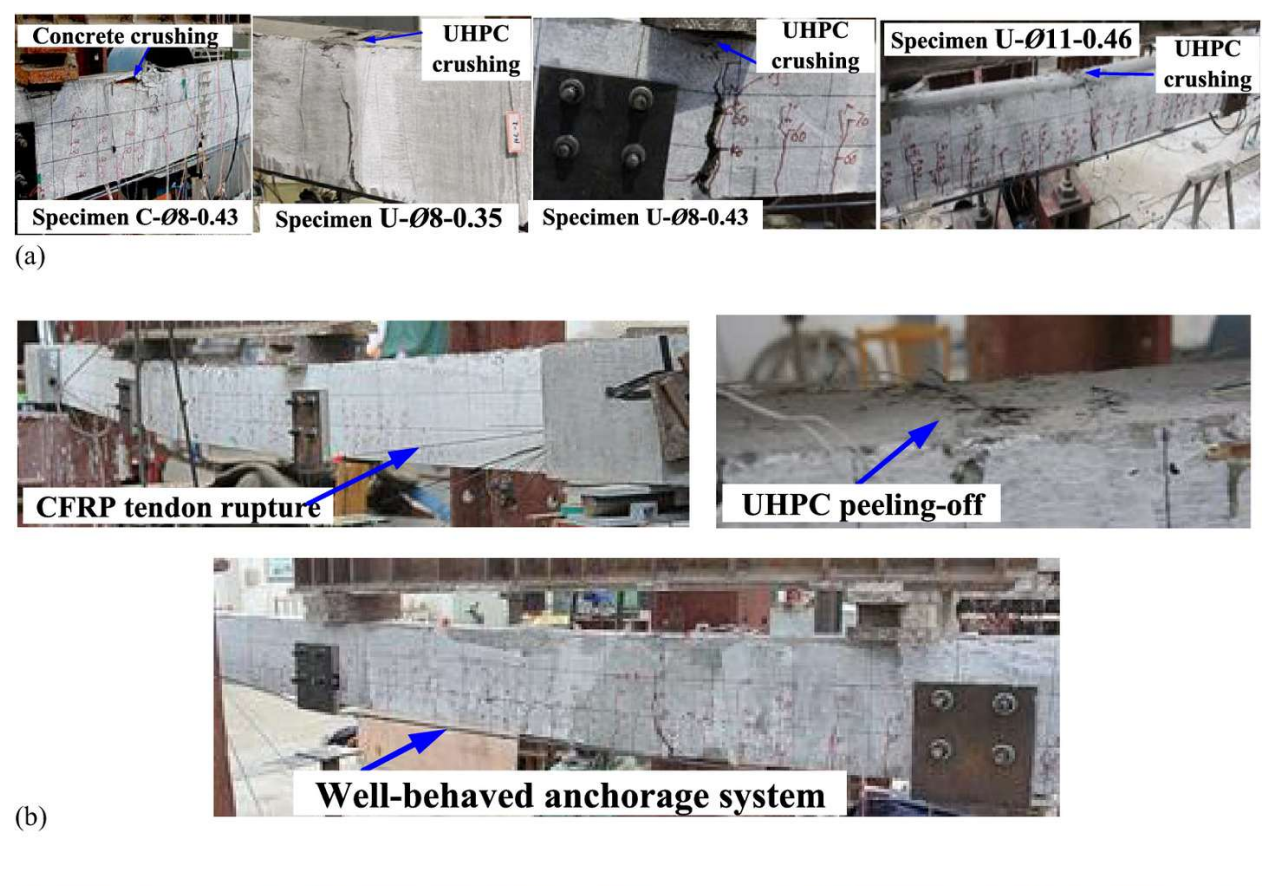




**Fig. 5**. Failure modes of all tested specimens: (a) Mode I: concrete crushing without the fracture of CC; (b) Mode II: UHPC peeling-off with CFRP tendon rupture (Specimen U-Ø8-0.62, UPF); and (c) Mode III: CFRP tendon rupture followed by UHPC crushing (Specimen U-Ø11-0.64, UCF).

## 5. Crack Pattern and Load-Maximum Crack Width Relationship

Fig. 6 shows the crack distributions of the tested specimens, where the numbers denote the applied load values measured by the load cell and the marked lines indicate the crack propagation path. The cracking load in Specimen C-Ø8-0.43 was 25% lower than that in Specimen U-Ø8-0.43 due to the higher tensile strength of the UHPC. A major crack developed in Specimen C-Ø8-0.43 and propagated almost across the entire section in the approaching failure

load of 75 kN, at which more uniform cracks in Specimen U-Ø8-0.43 propagated just up to a height of 150 mm due to the superior tensile resistance of the UHPC. Furthermore, as the initial pretension force decreased, under the same applied force (90 kN), the crack propagated upward to a height of 240 mm in Specimen U-Ø8-0.35, whereas it propagated to a height of 160 mm in Specimen U-Ø8-0.43. Therefore, increasing the initial prestressing forces in the CFRP tendons caused the lower cracks to occur uniformly along the beam span, thereby increasing the stiffness and bearing capacity. Additionally, as the diameter of the external CFRP tendon increased, the prestressed beam exhibited a higher load-bearing capacity. Beyond the yielding stage, the external CFRP tendon began to share more load, and the UHPC beam continued to experience a larger deflection, resulting in more crack development. The development and propagation of a larger tensile strain along the steel reinforcements resulted in numerous denser cracks, which were more pronounced at the highest initial prestressing force and larger-diameter CFRP tendons, indicating the full use of the high tensile strength of both the CFRP tendons and UHPC.

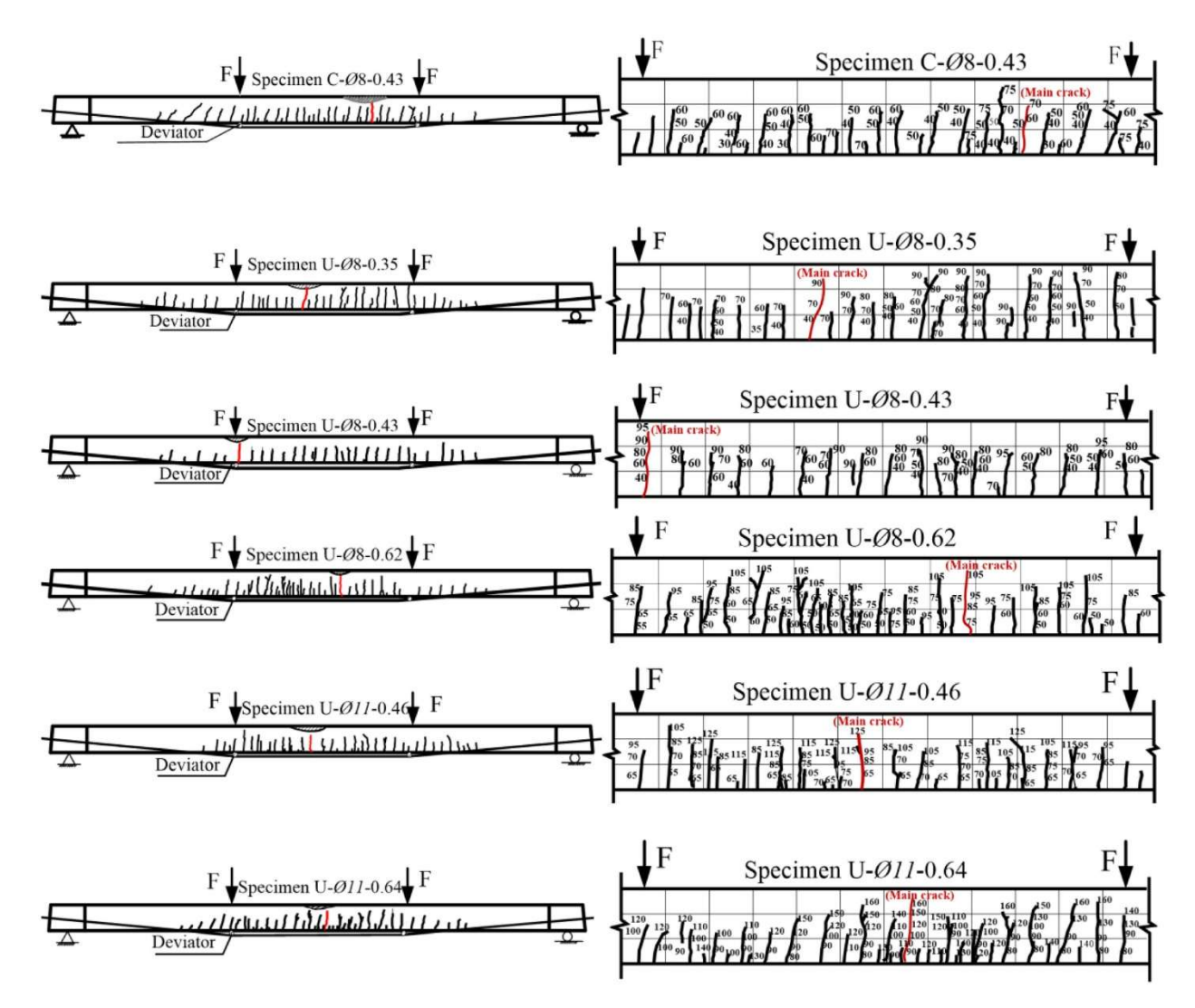


Fig. 6. Crack pattern of specimens.

Fig. 7 shows the evolution of the maximum crack width with an increasing applied load. Note that the curve of Specimen U-Ø8-0.43 is different from that of other specimens because the concrete near the deviator suddenly cracked in Specimen U-Ø8-0.43, approaching the yielding of steel reinforcement. Unexpectedly, major premature cracks inhibited the development and propagation of narrow and dense cracks in the UHPC. For the 8-mm-diameter CFRP tendon specimens shown in Fig. 7, the maximum crack width increased slowly before the major crack near the loading point occurred when a higher initial pretension stress was exerted. Subsequently, owing to the gradual sizzling sound heard between the deviator and the aluminum sheet coated on the CFRP tendons, the measurement of maximum crack width was stopped. This

difference in curve shape is attributed to a premature major crack near the loading point, which affects the flexural deformation of the beam.

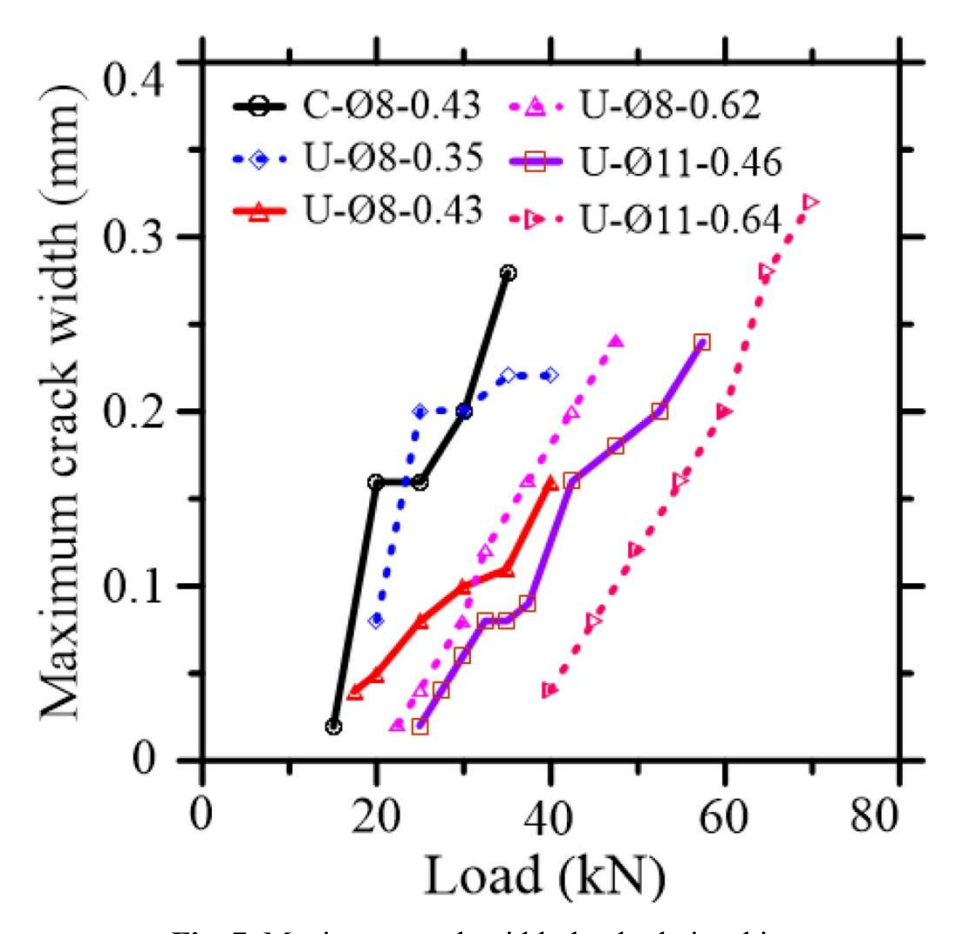


Fig. 7. Maximum crack width—load relationship.

Specimen C- $\emptyset$ 8-0.43 shows the most rapid increase in the crack width, especially after the yielding of the internal steel reinforcements, reaching up to 0.3 mm. By comparison, Specimen U- $\emptyset$ 8-0.43 showed a slower increasing trend and achieved 0.15 mm at 90%  $P_u$  ( $P_u$  is the ultimate load). In addition, although the initial prestressing force in Specimen U- $\emptyset$ 8-0.62 was 89% lower than that of Specimen U- $\emptyset$ 11-0.64, a similar rate of increase in crack width was observed. At an applied load of 40 kN, the maximum crack width in the two specimens reached 0.2 and 0.04 mm, respectively. Thus, increasing the tendon diameter resulted in higher total pretension forces acting on the anchorages and deviators, significantly delaying the crack opening. The increased load-sharing capacity of the externally prestressed CFRP tendons produced a higher vertical reaction force owing to a larger diameter and higher initial prestressing, hence reducing the stress

in the inner steel reinforcements, lowering the crack opening. Thus, UHPC operating with a higher prestressing force in the CFRP tendons contributes to a denser and lower crack pattern.

# 6. Load-Deflection Response

Table 4 lists the test results corresponding to the critical loading points, and Fig. 8 shows the load midspan deflection curves of all tested beams. The load-deflection curves exhibited three stages, characterized by the cracking point  $P_{cr}$ , yielding point  $P_y$ , and ultimate point  $P_u$ . Prior to cracking, the load linearly increased with the increasing midspan deflection. After the concrete cracking, the load-deflection curve was initiated with reduced flexure stiffness. When the internal steel reinforcements yielded, the load-deflection curve entered the third stage with a more rapid increase in the deflection. Owing to the linear elastic property, the CFRP tendon still shared the increasing load during the third stage, whereas steel tendons could not bear more loads.

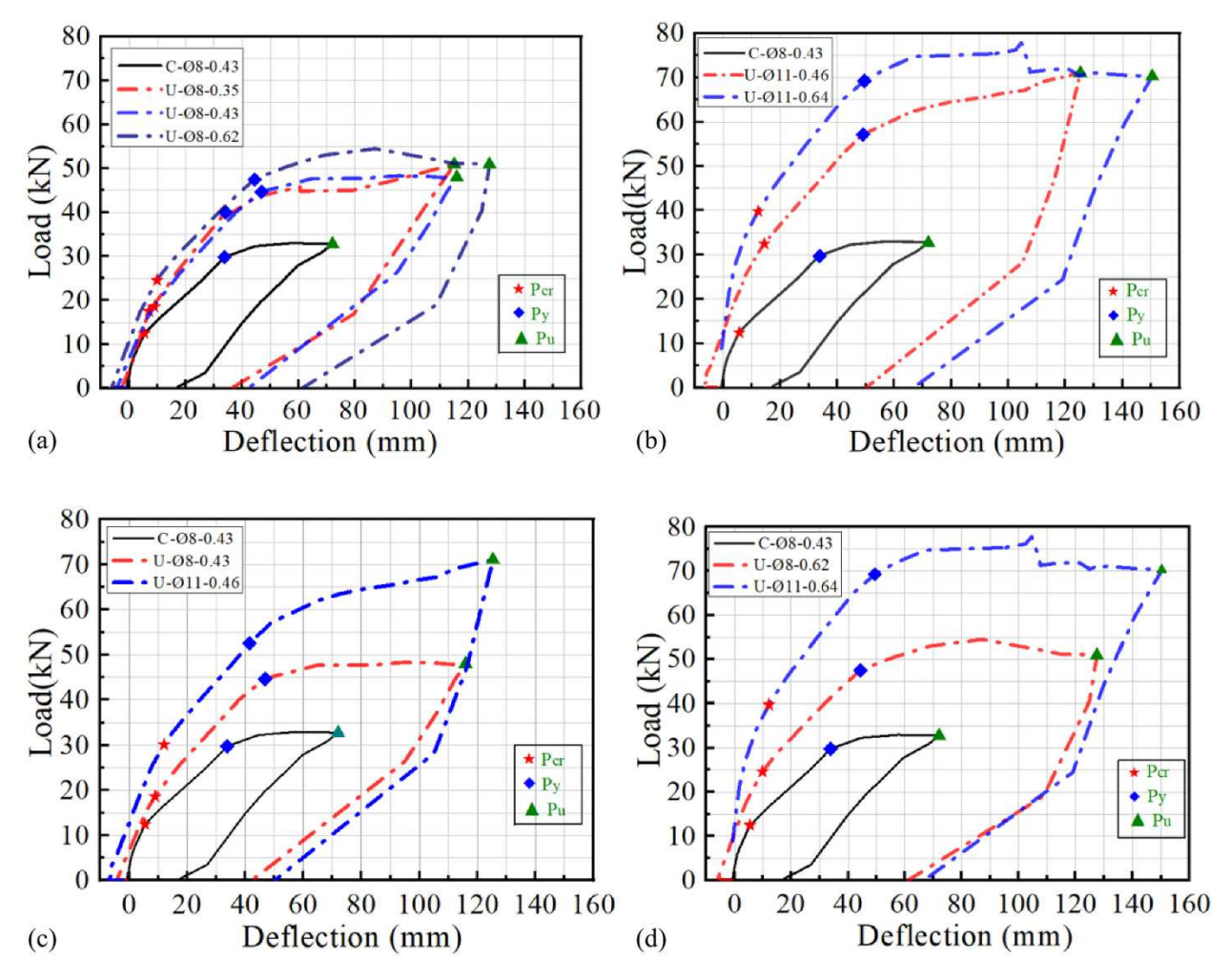


**Fig. 8**. Load–deflection relationships affected by various parameters: (a) effect of initial prestress degree (Ø8); (b) effect of initial prestress degree (Ø11); (c) effect of CFRP tendon diameter (0.43); and (d) effect of CFRP tendon diameter (0.64).

Table 4. Summary of the test results

		Elastic phase			Cracking-to-yielding			Yielding-		
Specimen ID	Failure modes	P <sub>cr</sub> (kN)	f <sub>cr</sub> (mm)	Δσ <sub>pc</sub> (MPa)	<i>P<sub>y</sub></i> (kN)	<i>f<sub>y</sub></i> (mm)	Δσ <sub>py</sub> (MPa)	P <sub>u</sub> (kN)	<i>f<sub>u</sub></i> (mm)	
C-Ø8-0.43	СС	30	8.6	58	60	35.1	193	75	77.6	
U-Ø8-0.35	СС	35	10.9	63	80	37.4	202	102	112.3	
U-Ø8-0.43	СС	40	11.5	57	89	46.8	267	106	116.3	
U-Ø8-0.62	UPF	55	13.7	63	95	44.4	243	110	127.9	
U-Ø11- 0.46	CC	65	14.4	76	105	41.4	178	139	128.6	
U-Ø11-	UCF	80	15.6	74	139	49.5	197	163	150.9	

Note: CC = concrete crushing failure; UPF = UHPC peeling off and CFRP tendon fracture; UCF = UHPC crushing and CFRP tendon fracture; and  $P_{cr}$ ,  $P_y$ , and  $P_u$  = cracking, yielding, and ultimate loads, respectively, and the corresponding deflections are labeled as  $f_{cr}$ ,  $f_y$ , and  $f_u$ , respectively. The stress increments in the external CFRP tendon at the cracking, yielding, and ultimate loads are marked as  $\Delta \sigma_{pc}$ ,  $\Delta \sigma_{py}$ , and  $\Delta \sigma_{pu}$ , respectively.

Fig. 9 shows the load-strain relationship in the steel reinforcement. The steel reinforcements in all the specimens reached their yielding strain. After concrete cracking, the strain in the steel reinforcement increased more slowly as the prestressing force increased, implying that the external CFRP tendon shared a higher force with increasing deflection.

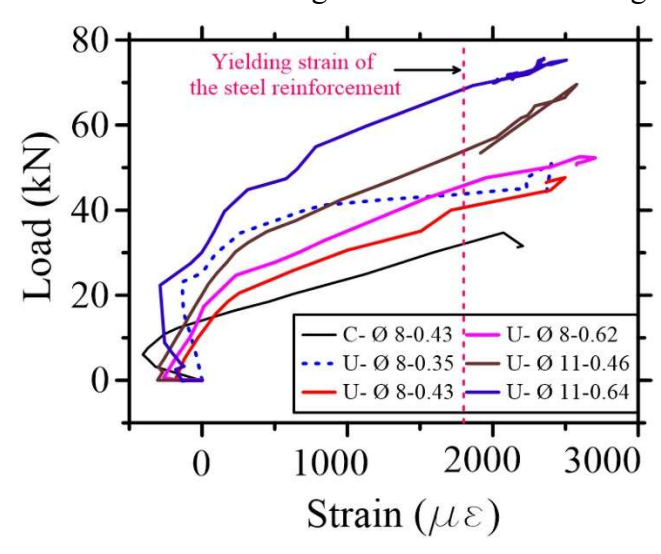


Fig. 9. Load-strain in the steel reinforcement relationship

## 7. Effect of Concrete Strength

Fig. 8(a) shows that Specimen U-Ø8-0.43 had 33% and 50% higher cracking and ultimate strengths, respectively, than Specimen C-Ø8-0.43 because of the higher compressive and tensile strengths of the UHPC. Previous findings by Sturm et al. (2020) indicated that the load capacity of prestressed concrete beams using steel tendons was 36% lower than that of beams with external CFRP tendons. Hence, the UHPC beams prestressed with CFRP tendons exhibited approximately 104% higher ultimate loads than the NC beams prestressed with steel tendons. Additionally, compared with the findings of Wang et al. (2024), under approximate prestress levels, the UHPC beams cracked at approximately 38% of the ultimate loads, which was higher

than the 24% in the NC beams prestressed with steel strands. This indicates that the higher tensile strength of the UHPC beneficially increased the cracking resistance.

Table 4 also shows that the ultimate midspan deflection of Specimens C-Ø8-0.43 and U-Ø8-0.43 reached 77.6 and 116.3 mm, accounting for 1/65 and 1/43 of the effective span length, respectively. This implies that using UHPC operating with externally prestressed CFRP tendons can improve both the ultimate strength and deformability. Conventionally, a prestressed FRP– reinforced beam is governed by the serviceability limit state requirements owing to the low elastic modulus of the FRP bars (Elgabbas et al. 2017; El-Nemr et al. 2013). As seen in Table 4, Specimen U-Ø8-0.43 shows a 50% higher yielding load and 12% larger flexural stiffness than Specimen C-Ø8-0.43. This implies that UHPC expanded the service scope of the prestressed CFRP members by achieving greater structural deformability. This enhancement was due to the superior postcracking stiffness triggered by the presence of assumed uniformly distributed steel fibers bridging the cracks in the UHPC, which was beneficial for structural whole-dependent rather than section-dependent deformation. The load-deflection responses in Fig. 8 show that beyond the yielding stage, relative to EPC beams with CFRP tendons, lower nonlinear decreasing trends in the beam's stiffness were observed for EPU beams with CFRP tendons owing to much less compressive damage in the concrete. In the NC beams prestressed with steel tendons, steel tendon yielding resulted in significant losses in beam stiffness, which were largely overcome by the prestressed CFRP tendon-reinforced UHPC beams. As suggested by GB 50608 (GB 2010), the FRP-reinforced beam at the serviceability limit state recommended an allowable deflection of L/200 (L is the beam span), which could allow a more relaxed deflection of L/115based on the test results in this study.

As observed by Wu et al. (2021), inelastic deformations due to concrete crushing lent a degree of ductility and the presence of steel fibers improved the postcracking stiffness due to their crackbridging capacity. When the external prestressed CFRP tendon ruptured, there was no significant reduction in the applied loads in this study. Compared with the findings of Sturm et al. (2020), the load decreased to between 68% and 77% of the peak load for pretensioned UHPC beams with steel tendons, and the linear stress increment property for the CFRP tendon compensated for

the load decrease and stiffness reduction triggered by the steel tendon yielding and the pulling out of the steel fibers.

### 8. Effect of Prestress Level

As observed from Fig. 8(b) and Table 4, when the UHPC was crushed, the cracking, yielding, and ultimate loads increased by 14%, 12%, and 4%, respectively, as the prestressing force increased by 21% (Specimens U-Ø8-0.43 and U-Ø8-0.35). The corresponding midspan deflections increased by 6%, 12%, and 4%, respectively. This phenomenon indicated that the compressive plasticity of the UHPC was activated to balance the tensile strain-hardening of the UHPC and higher stress in the CFRP tendons, resulting in a larger ultimate deformation and bearing capacity. Compared with Specimen U-Ø8-0.43, as the initial prestress level increased by 44% in Specimens U-Ø8-0.62, the failure changed from slight crushing of the UHPC to the UHPC peeling off with the tensile fracture of CFRP tendons. The cracking load increased by 38%, whereas the yield and ultimate loads increased by only 6% and 4%, respectively. Accordingly, the cracking and ultimate midspan deflections increased by 18% and 10%, respectively, whereas the yielding midspan deflections decreased by 5%. Thus, a balanced prestress level is required to clarify the boundaries between UHPC crushing and CFRP tendon rupture. A higher initial prestress force in the CFRP tendons enabled enhanced cracking and ultimate loads for the UHPC beams by employing a wider UHPC domain and achieving larger structure-dependent deformability, which was different from the brittle and local failure in the NC members.

Similarly, in the specimens prestressed with 11-mm-diameter CFRP tendons, as the prestress force increased by 41%, the cracking, yielding, and ultimate loads increased by 23%, 32%, and 17%, respectively. The corresponding midspan deflections increased by 9%, 19%, and 17%, respectively. Unlike the significant losses in flexural stiffness owing to the yielding of prestressed NC beams with steel tendons (Le et al. 2020), the EPU beams with CFRP tendons still exhibited an increased postyielding strength. This indicates that the use of UHPC largely relieved the serious damage occurring in the NC specimens, thereby improving the postyielding stiffness.

For the NC and UHPC crushing failure, the ultimate tensile strength of the CFRP tendon reached approximately 61% and 73% of its nominal breaking strength, respectively. In comparison, the CFRP tendon ruptured at its nominal breaking strength, which was higher than the 78% proportion observed by Le et al. (2020).

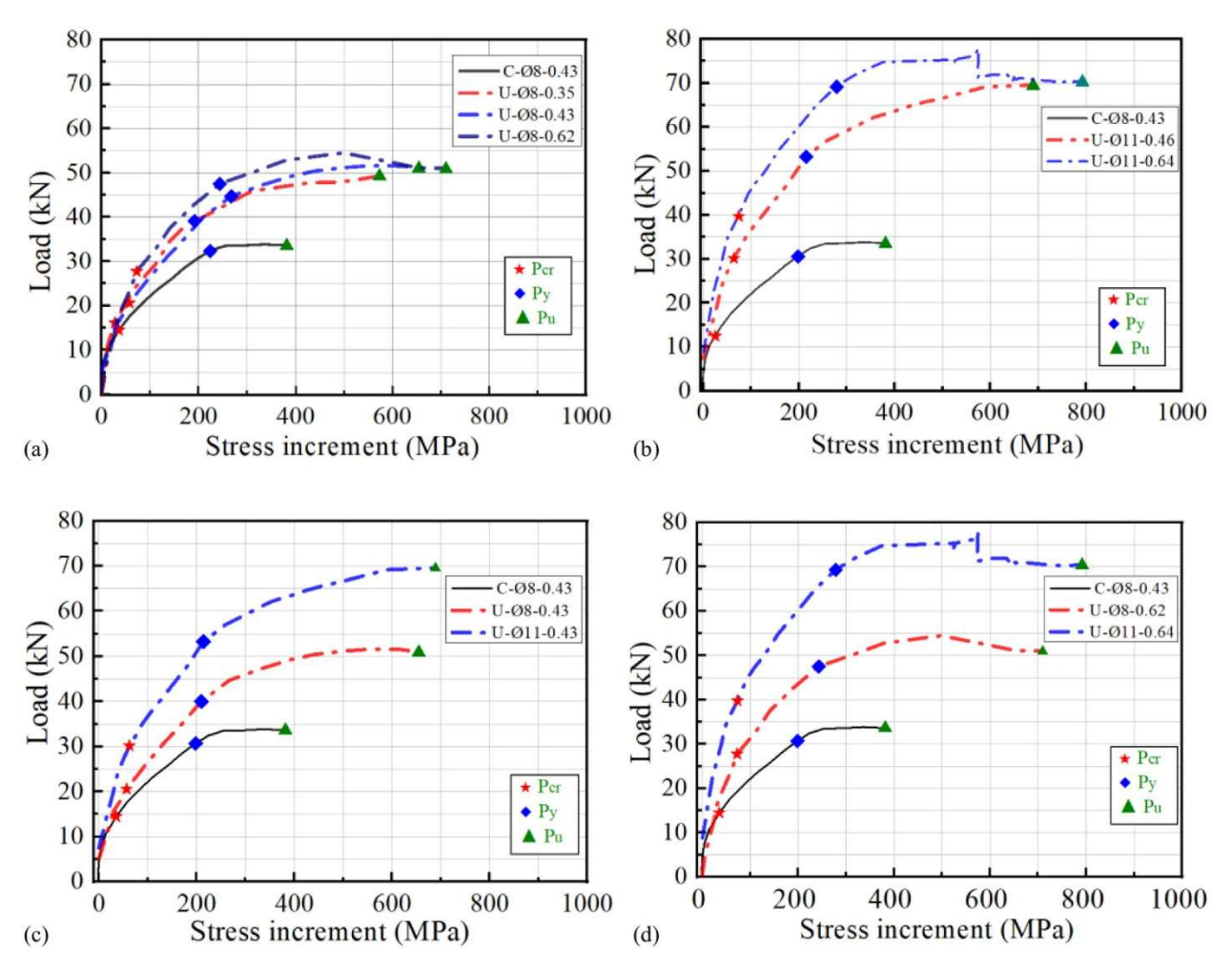
## 9. Effect of Prestressing Tendon Diameter

Fig. 6 shows that the UHPC in Specimen U-Ø11-0.64 was crushed more seriously with lateral bending than Specimen U-Ø8-0.62. As shown in Figs. 8(c and d), the ultimate tensile strength of the CFRP tendon increased by 77% as its diameter increased from 8 to 11 mm, which was higher than the tested ultimate load increases of 31% and 48%, respectively. This is because the higher prestressing forces resulting from the larger diameter of the CFRP tendons enabled premature plastic deformation in the UHPC along the entire span length, resulting in a rapidly increased deflection.

Meanwhile, as the CFRP tendon diameter increased, the flexural stiffness at the cracking, yielding, and ultimate loads increased by 31%, 33%, and 19%, respectively, at a prestress level of approximately 0.43, whereas increases of 27%, 31%, and 25%, respectively, were observed at a prestress level of 0.63. This increased flexural stiffness occurred because increasing the external tendon diameter produced a higher equivalent vertical reaction force and thus compensated for some of the midspan deflection. In addition, a larger prestress force inhibited crack propagation (Fig. 6) and improved the effective section area along the entire span, leading to a larger structural stiffness. Compared to the NC specimens, the characteristic stiffness increased by 16%, 25%, and 10%, respectively, for the 8-mm-diameter CFRP specimens, whereas respective improvements of 30%, 49%, and 12% were observed for the 11-mm-diameter CFRP specimens. This indicates that the larger-diameter CFRP tendons produced higher prestressing forces that beneficially increased the global stiffness and significantly improved the yield and ultimate stiffness relative to EPC beams with CFRP tendons. Thus, a smaller number of larger-diameter rather than smaller-diameter external prestressing CFRP tendons enabled both a higher ultimate bearing capacity and stronger stiffness.

## 10. Load-Stress Increment Response

Fig. 10 shows the relationship between the stress increments ( $\Delta f_{ps}$ ) in the external CFRP tendons and the applied loads, which were similar to the load–deflection curves, characterized by three stages.



**Fig. 10**. Comparison of load–stress increment relationships for all tested beams: (a) effect of initial prestress degree (Ø8); (b) effect of initial prestress degree (Ø11); (c) effect of CFRP tendon diameter (0.43); and (d) effect of CFRP tendon diameter (0.64).

## 11. Effect of Concrete Strength

As shown in Fig. 10(a), a higher stress increase occurred in the UHPC specimens than in the NC specimens, particularly after the yielding load. It can be observed from Figs. 6 and 7 that the wider cracks opened and propagated along the height, resulting in smaller section stiffness and

thus increased deflection under a lower yielding load. Ultimately, the stress increase in the NC specimen was only 60% of that in the UHPC specimen. Beyond the yield point, the external CFRP tendons had a prominent influence on the structural resistance, as expected, and the distinction between the NC and UHPC series specimens was appreciable because the smaller concrete strength and lower deformability of the NC were incapable of supporting further global deflection, which was confirmed by Ghallab and Beeby (2005). This suggests that UHPC operating with CFRP tendons can be used to develop longer-span bridges with superior deformability.

### 12. Effect of Prestress Level

In Fig. 10(a), relative to Specimen U-Ø8-0.35, as the prestress level increased, the ultimate stress in the CFRP tendon increased by 10% and 19%, respectively. This was because a higher initial prestress force significantly delayed the crack propagation and yielding of the internal steel reinforcements, which led to more UHPC engaging in the strain-hardening phase with more steel fibers bridging subtle cracks and developing a longer plastic hinge in the internal steel reinforcements.

For the 11-mm-diameter CFRP tendon specimens, as shown in Fig. 10(b), the stress increment influenced by the prestress level was more pronounced. As the initial prestress force increased, the cracking, yielding, and ultimate loads increased more rapidly than the tendon stress owing to higher flexural stiffness. Beyond the yielding load, the slope of the curve for Specimen U-Ø11-0.64 was first higher and then lower than that of Specimen U-Ø11-0.46 because the longitudinal fibers in the CFRP tendon fractured progressively until the full rupture of the CFRP tendon.

A higher initial prestress increased the flexural stiffness of the beam. Considering the sudden brittle rupture of the CFRP tendon, the initial prestress level was recommended to be no more than  $0.62 f_{pu}$  to favor the UHPC crushing as an indicator of ductility.

# 13. Effect of Prestressing Tendon Diameter

In Figs. 10(c and d), as the prestress increased in a larger-diameter CFRP tendon, the load increased more rapidly due to higher stiffness assistance from the external tendons. Ultimately, an approximate stress increment was observed for the same failure mode. Overall, the larger the

global deformation of the UHPC specimen, the higher the ultimate tensile strength of the external tendon. During the postyielding stage, the stress increment accounted for 50%, 66%, 58%, 65%, 74%, and 75% of the total stress increment, respectively, for Specimens C-Ø8-0.43, U-Ø8-0.35, U-Ø8-0.43, U-Ø8-0.62, U-Ø11-0.46, and U-Ø11-0.64. This indicated that the CFRP tendons experienced >50% deformation in the third stage. For CC failure in Specimens U-Ø8-0.43 and U-Ø11-0.46, approximate ultimate stress (1,519 and 1,566 MPa) occurred in the CFRP tendons, while their total tensile stresses in Specimens U-Ø8-0.62 and U-Ø11-0.64 reached 1,978 and 2,026 MPa, respectively, which were close to the fracture strength of CFRP tendons and exceeded the yielding stress of the common steel strand, which is 1,860 MPa. Hence, using the UHPC and CFRP tendons instead of NC and steel strands is a perfect alternative for improving strength.

## 14. Stress Increment-Midspan Deflection Response

Fig. <u>11</u> shows that the stress increment linearly increases with the midspan deflection throughout the entire loading phase, which agrees with previously reported results (<u>Harajli 2006</u>; <u>He and Liu 2010</u>).

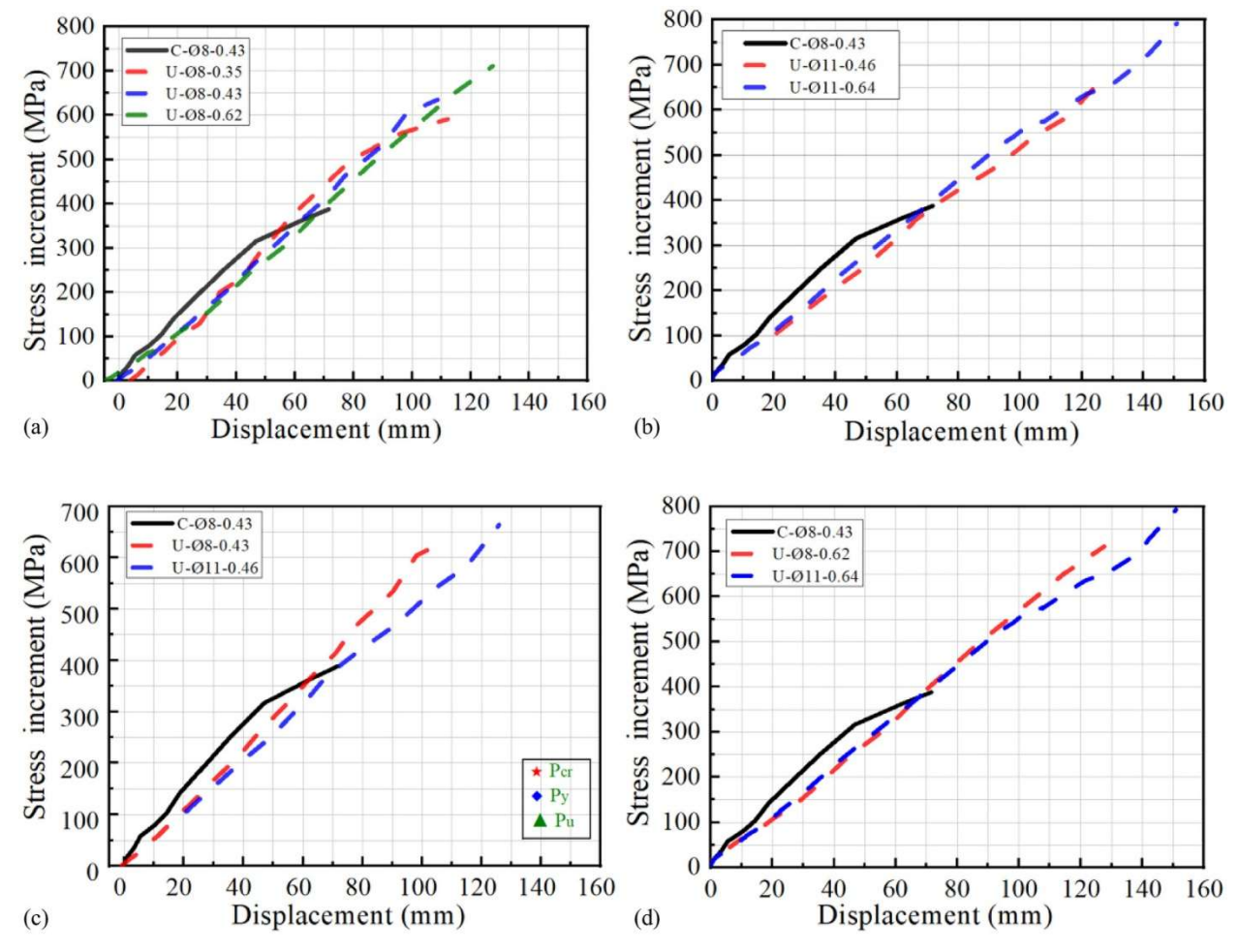


**Fig. 11**. Comparison of stress increment–deflection relationships: (a) effect of initial prestress degree (Ø8); (b) effect of initial prestress degree (Ø11); (c) effect of CFRP tendon diameter (0.43); and (d) effect of CFRP tendon diameter (0.64).

Fig. 11(a) shows that Specimen U-Ø8-0.43 had a smaller stress increment than Specimen C-Ø8-0.43 at the same midspan deflection because of the greater extreme compression strain and slower crack propagation of the UHPC, as discussed previously. However, non-prestressed reinforcements are considered to affect the crack distributions and ultimate external prestress tendon stress (Tao and Du 1985). By analogy, uniform steel fibers can be assumed to function as steel reinforcements to improve the brittle characteristics and enhance the structural stiffness, as stated previously.

Fig. <u>11(a)</u> shows that increasing the prestress level reduces the curve slope accordingly, owing to the higher structural flexural stiffness. Fig. <u>11(b)</u> shows a plot of the tendon stress increment—

midspan deflection relationship for the 11-mm-diameter CFRP tendon specimens. Relative to Specimen U-Ø11-0.46, the stress increment in Specimen U-Ø11-0.64 was initially similar and then increased more rapidly until its final reduced growth rate because the UHPC bore a high axial compressive strain shortening the axial length between two anchorage ends at the UHPC crushing when the specimen changed from compression to tensile failure (i.e., CC to UCF) under a higher initial prestress force. Thus, the stress increment ratio tended to decrease at a prestress level of 0.64. Additionally, Figs. 11(c and d) indicate that as the external tendon diameter increased, the stress increased more slowly, owing to the lower stress required to balance the compressive force. Previous findings (Le et al. 2020; Wang et al. 2015) revealed that a draped angle of 3° in the external tendons led to a decrease in the ultimate tensile strength by approximately 10%, and that the shear stress on the CFRP tendons at the deviators might reduce the fracturing stress. In this study, 11- and 8-mm-diameter CFRP tendons ruptured at a 4% lower ultimate tensile strength, validating the effectiveness of the proposed deviators.

# 15. Ductility

The ductility coefficient is defined as the ultimate-to-yielding deflection ratio listed in Table 4. For Specimens C-Ø8-0.43 and U-Ø8-0.43, the ductility coefficients were calculated as 2.21 and 2.48, indicating that using UHPC instead of the NC increased the structural ductility because the major crack in the NC extended upward to the top compression zone quickly, with a smaller ultimate deformation and lower neutral axis because of lower compressive strength and strain in the NC specimens. Additionally, previous studies have shown that for pretensioned UHPC beams, the average ductility factor for CFRP-reinforced beams was 66% of that for specimens with prestressed steel tendons (Sturm et al. 2021). This implies that the EPU beams with CFRP tendons had higher ductility than the EPC beams with CFRP tendons but lower ductility than the UHPC members prestressed with steel tendons.

The ductility coefficients of all the UHPC specimens were higher than those of the NC specimens. In Specimens C-Ø8-0.35 and U-Ø8-0.43, increasing the prestress level decreased the ductility by 17% due to a higher axial compression ratio. As the pretension stress increased in the 8- and 11-mm-diameter CFRP tendons, the ductility coefficient decreased from 3.0 to 2.88 and from 3.1 to 3.05, respectively. The brittleness (without a clear failure symbol) in previous EPC

beams with CFRP tendons was improved effectively (<u>El Meski and Harajli 2015</u>). In this study, the external CFRP tendons ruptured, accompanied by gradual fracturing of the longitudinal carbon fiber rather than sudden rupture of an entire cross section, providing a clear failure signal.

As the external tendon diameter increased, for the concrete crushing failure, the ductility coefficient of Specimen U-Ø8-0.43 was 25% higher than that of Specimen U-Ø11-0.46, whereas only a 6% improvement was found in the ductility of Specimen U-Ø11-0.64 relative to Specimen U-Ø8-0.62. This means that for a prestress level below 0.62, increasing the tendon diameter could significantly increase the structural ductility because a larger-diameter external CFRP tendon can provide a higher tensile resistance and share higher external loads, thereby delaying the excessive deformation of the steel reinforcements.

Compared with steel tendons, the external prestressed CFRP tendons ruptured at a relatively low strain level of approximately 0.013 in this study. The lower deformability of the CFRP tendon resulted in a brittle failure response of the structure. To mitigate this adverse effect and consequently improve the structural ductility, using both steel and CFRP tendons or steel-CFRP composite rebars as external prestressing tendons in UHPC beams could be an alternative.

## **Evaluation of the Test Results**

The stress increment in the externally prestressed tendons is regarded as an important factor in determining the ultimate bending resistance of the EPC beams. The possible calculation models are provided by ACI PRC-440.4-04 (ACI 2004) and AASHTO (2020).

ACI PRC-440.4-04 notes that the stress in the CFRP tendons could be predicted based on the strain reduction coefficients by establishing the correlation between the bonded and unbonded prestressing systems, thereby simplifying the global deformation analysis to the section analysis. In this approach, two parameters were considered for obtaining the reduction coefficients at failure that is, the loading modes and the span-to-depth ratio. Then, the ultimate stress of the external prestress tendon ( $f_{ps1}$ ) can be predicted by the following equation:

$$f_{ps1} = f_{pe} + \Omega_u E_{\text{FRP}} \xi_{cu} \left(\frac{d_p}{c} - 1\right) \frac{L_1}{L_2} \tag{1}$$

where  $f_{pe}$  = initial effective prestress in the tendon;  $E_{FRP}$  = elastic modulus of the prestressing FRP tendon; L = span length;  $L_1$  = sum of load spans containing the tendon considered;  $\zeta_{cu}$  = failure strain of concrete in compression;  $L_2$  = length of the tendon between the anchorages; and  $\Omega_u$  = ratio of strain increase in the unbonded tendon to that of the equivalent bonded tendon at the section of maximum moment where  $\Omega_u = 3/(L/d_p)$  for uniform or third-point loading and  $\Omega_u$  =  $1.5/(L/d_p)$  for one-point midspan loading.

AASHTO (2020) specifies the following expression to calculate the ultimate stress in the unbounded tendons ( $f_{ps2}$ ):

$$f_{ps2} = f_{pe} + 6,200 \left(\frac{d_{ps} - c}{l_e}\right) \tag{2}$$

where  $d_{ps}$  = distance from the extreme fiber to the centroid of the prestressing tendons; c = neutral axis depth of the section; and  $l_e = L/(1 + N/2)$ , where L = length of the tendon between the anchorages and N = number of support hinges required to form a flexural mechanism that is crossed by the tendon.

After the ultimate tensile strength of the external tendon and depth of the compression zone were obtained, the ultimate moment  $(M_u)$  of EPC beams with CFRP tendons was calculated based on the sectional internal force balance by the following equations:

$$f_{ps}A_p + f_yA_s = f_{ck}bc (3)$$

$$M_u = f_{ps}A_p(d_{ps} - c/2) + f_yA_s(h_s - c/2)$$
(4)

where  $f_{ps}$  = ultimate stress in the prestressing tendon;  $A_p$  = area of the external prestress tendon;  $f_y$  = yielding stress of the internal tendon;  $A_s$  = area of the prestressing tendon;  $d_{ps}$  =

distance from the extreme fiber to the centroid of the internal tendons; c = neutral axis depth of the section;  $h_s$  = distance from the extreme fiber to the centroid of the prestressing tendons;  $f_{ck}$  = standard value of the concrete compressive strength; and b = beam width.

As shown in the failure modes, the peeling-off failure of a small UHPC domain without completely crushing the UHPC was considered to have reached its peak strain, whereas the outermost fibers in the CC and UCF were thought to have reached the ultimate compressive strain of the UHPC. The tensile strengths of CFRP tendons in Eqs. (1)–(4) can be derived using simple iterative steps. A comparison of the experimental and theoretical results is presented in Table 5.

**Table 5**. Comparison between the test results and theoretical capacity

Specimen	Test results		ACI PRC-440.4-04				AASHTO (202		
	f <sub>test</sub> (MPa)	F <sub>test</sub> (kN)	f <sub>psl</sub> (MPa)	f <sub>psl</sub> /f <sub>test</sub>	<i>F<sub>uīl</sub></i> (kN)	F <sub>ul</sub> /F <sub>test</sub>	f <sub>ps2</sub> (MPa)	f <sub>ps2</sub> /f <sub>test</sub>	<i>F<sub>u2</sub></i> (kN)
C-Ø8-0.43	388	38	405	1.04	38	1.00	270	0.69	35
U-Ø8-0.35	589	51	526	0.89	43	0.84	310	0.53	39
U-Ø8-0.43	643	53	700	1.09	46	0.86	309	0.48	41
U-Ø8-0.62	702	55	781	1.11	54	0.98	308	0.44	47
U-Ø11- 0.46	690	70	500	0.72	60	0.86	309	0.45	56
U-Ø11-	792	82	691	0.87	76	0.93	308	0.39	64

Note:  $f_{\text{test}}$  = tested ultimate stress in the external CFRP tendon; and  $F_{u1}$  and  $F_{u2}$  = failure loads, calculated as per ACI PRC-440.4-04 and AASHTO (2020), respectively.

As listed in Table 5, ACI PRC-440.4-04 predicted the ultimate stress in the CFRP tendon and the failure loads more accurately than AASHTO (2020). In addition to the compressive zone depth and external prestress tendon depth-to-beam span ratio considered in AASHTO (2020), the ultimate tensile stress of the external CFRP tendon in ACI PRC-440.4-04 is also related to the ultimate compressive strain of UHPC, which can accurately quantify the structural deformability

at failure, especially for EPU beams with CFRP tendons. The bond-reduction coefficient in Eq. (1) warrants further validation.

### **Conclusions**

This study investigated the flexural performance of EPU beams with CFRP tendons from six simply supported beams, considering the influence of concrete strength, initial prestressing level, and CFRP tendon diameter. The following conclusions were drawn based on the test results:

- 1. As the initial pretension stress increased, the failure mode of the EPU beams with CFRP tendons changed from UPF to UCF. The EPU beams with CFRP tendons specimens showed a crack width that was 0.2 mm smaller than the 0.3 mm crack width developed in EPC beams with CFRP tendons because of the superior cracking resistance of UHPC. Increasing the CFRP tendon diameter from 8 to 11 mm had a more significant influence on the development of denser and shorter distributed cracks than increasing the initial prestressing force, in which the maximum crack width was reduced from 0.2 to 0.04 mm.
- 2. Replacing NC with UHPC improved the ultimate strength by 50% and increased the ultimate midspan deflection from 1/65 to 1/43 of the effective span length. Meanwhile, a 33% larger yielding deflection was achieved under a 50% higher yielding load, owing to the presence of the steel fibers, which were assumed to be uniformly distributed, inhibiting the crack opening and enhancing the postcracking stiffness. The multiple dense crack distributions were compatible with the structural whole-dependent deformation in the EPU beams with CFRP tendons.
- 3. Increasing the initial prestress by 21% and 44% in the 8-mm-diameter CFRP tendons led to 14% and 38% higher cracking loads, respectively, by employing more UHPC to share the strength, and the influence of this effect more significant as the CFRP tendon diameter increased. Using UHPC instead of NC with the CFRP tendon relieved serious concrete damage and increased the postyielding stiffness.
- 4. The ultimate load increased less proportionally than the cross-sectional area of the CFRP tendon because the generated premature plastic deformation under high prestress resulted in a

rapidly increasing deflection. The flexural stiffness was enhanced more significantly than the ultimate loads as the CFRP tendon diameter increased, with fewer larger-diameter CFRP tendons enabling both higher ultimate strength and stiffness.

5. The stress increment in the external CFRP tendon increased linearly with the midspan deflection and mostly occurred during the postyielding stage. The higher strength and deformability of UHPC compared to NC resulted in a larger stress increment in the CFRP tendons. Increasing the initial prestress beyond the level of 0.62 and the CFRP tendon diameter led to more UHPC engaging in strain hardening and thus a higher stress increment, which provided a higher ductility by assisting in delaying the excessive deformation of the non-prestressed steel reinforcements.

Based on the findings of this study, it is suggested that the prestressing level in the external CFRP tendon for UHPC members should not exceed  $0.62f_{pu}$  to avoid rupture of the CFRP tendon. Further studies are required to determine the optimum prestressing level for EPU beams with CFRP tendons. Several specimens were tested at the same deviator angle of 4.7°. Future research is warranted to study the effects of various deviator angles of the CFRP tendon on both the proposed anchorage and deviator systems.

# **Data Availability Statement**

All data, models, or codes that support the findings of this study are available from the corresponding author upon reasonable request.

# Acknowledgments

The authors gratefully acknowledge the financial support provided by the National Key Research and Development Program (2023YFB3711603), the National Science Foundation of China (52308175), the Jiangsu Province Youth Science and Technology Talent Support Project (JSTJ-2023-JS002, General Project BK20241872), and the Jiangsu Province Key Technology Project of Transportation (2024QD10).

### References

AASHTO. 2020. AASHTO LRFD bridge design specifications. 9th ed. Washington, DC: AASHTO.

ACI (American Concrete Institute). 2004. *Prestressing concrete structures with FRP tendons* (reapproved 2011). ACI PRC-440.4-04. Farmington Hills, MI: ACI.

Dall'Asta, A., L. Ragni, and A. Zona. 2007. "Simplified method for failure analysis of concrete beams prestressed with external tendons." *J. Struct. Eng.* 133 (1): 121–131. https://doi.org/10.1061/(ASCE)0733-9445(2007)133:1(121).

Elgabbas, F., E. A. Ahmed, and B. Benmokrane. 2017. "Flexural behavior of concrete beams reinforced with ribbed basalt-FRP bars under static loads." *J. Compos. Constr.* 21 (3): 04016098. https://doi.org/10.1061/(ASCE)CC.1943-5614.0000752.

El Meski, F., and M. Harajli. 2015. "Evaluation of the flexural response of CFRP-strengthened unbonded posttensioned members." *J. Compos. Constr.* 19 (3): 04014052. https://doi.org/10.1061/(ASCE)CC.1943-5614.0000516.

El-Nemr, A., E. Ahmed, and B. Benmokrane. 2013. "Flexural behavior and serviceability of normal- and high-strength concrete beams reinforced with glass fiber-reinforced polymer bars." *ACI Struct. J.* 110 (6): 1077–1087.

Elrefai, A., J. S. West, and K. A. Soudki. 2008. "Effect of overloading on fatigue performance of reinforced concrete beams strengthened with externally post-tensioned carbon-fibre-reinforced polymer tendons." *Can. J. Civ. Eng.* 35: 1294–1307. https://doi.org/10.1139/L08-070.

Fang, Z., R. Hu, R. Jiang, Y. Xiang, and C. Liu. 2020. "Fatigue behavior of stirrup free reactive powder concrete beams prestressed with CFRP tendons." *J. Compos. Constr.* 24 (4): 04020018. <a href="https://doi.org/10.1061/(ASCE)CC.1943-5614.0001027">https://doi.org/10.1061/(ASCE)CC.1943-5614.0001027</a>.

Gao, D., D. Fang, P. You, G. Chen, and J. Tang. 2020. "Flexural behavior of reinforced concrete one-way slabs strengthened via external post-tensioned FRP tendons." *Eng. Struct.* 216: 110718. https://doi.org/10.1016/j.engstruct.2020.110718.

GB (Guobiao Standards). 2010. *Technical code for infrastructure application of FRP composites*. GB 50608. Beijing: China Architecture and Building Press.

GB (Guobiao Standards). 2015. *Reactive powder concrete*. GB/T 31387-2015. Beijing: China Planning Press.

Ghallab, A., and A. W. Beeby. 2005. "Factors affecting the external prestressing stress in externally strengthened prestressed concrete beams." *Cem. Concr. Compos.* 27 (9): 945–957. https://doi.org/10.1016/j.cemconcomp.2005.05.003.

Grace, N. F., S. Sachidanandan, and S. Puravankara. 2006. "Behavior of prestressed concrete box-beam bridges using CFRP tendons." *PCI J.* 51: 26–41. https://doi.org/10.15554/pcij.03012006.26.41.

Harajli, M. H. 1993. "Strengthening of concrete beams by external prestressing." *PCI J.* 38 (6): 76–88. <a href="https://doi.org/10.15554/pcij.11011993.76.88">https://doi.org/10.15554/pcij.11011993.76.88</a>.

Harajli, M. H. 2006. "On the stress in unbonded tendons at ultimate: Critical assessment and proposed changes." *ACI Struct. J.* 103 (6): 803–812.

He, Z.-Q., and Z. Liu. 2010. "Stresses in external and internal unbonded tendons: Unified methodology and design equations." *J. Struct. Eng.* 136 (9): 1055–1065. https://doi.org/10.1061/(ASCE)ST.1943-541X.0000202.

Kato, T., and N. Hayashida. 1993. *Flexural characteristics of prestressed concrete beams with CFRP tendons*, 419–440. Vol. 138. Farmington Hills, MI: American Concrete Institute.

Kim, P., and U. Meier. 1991. "CFRP cables for large structures." In Proc., Advanced Composites Materials in Civil Engineering Structures, 233–244. Reston, VA: ASCE.

Le, T. D., T. M. Pham, H. Hao, and Y. Hao. 2018. "Flexural behaviour of precast segmental concrete beams internally prestressed with unbonded CFRP tendons under four-point loading." *Eng. Struct.* 168: 371–383. https://doi.org/10.1016/j.engstruct.2018.04.068.

Le, T. D., T. M. Pham, H. Hao, and H. Li. 2020. "Behavior of precast segmental concrete beams prestressed with external steel and CFRP tendons." *J. Compos. Constr.* 24 (5): 04020053. https://doi.org/10.1061/(ASCE)CC.1943-5614.0001059.

Le, T. D., T. M. Pham, H. Hao, and C. Yuan. 2019. "Performance of precast segmental concrete beams posttensioned with carbon fiber-reinforced polymer (CFRP) tendons." *Compos. Struct.* 208: 56–69. https://doi.org/10.1016/j.compstruct.2018.10.015.

Lee, C., S. Shin, and S. Lee. 2015. "Modelling of load–deflection of concrete beams internally prestressed with unbonded CFRP tendons." *Mag. Concr. Res.* 67: 730–746. <a href="https://doi.org/10.1680/macr.14.00367">https://doi.org/10.1680/macr.14.00367</a>.

MOHURD (Ministry of Housing and Urban-Rural Development). 2016. *Technical specification* for concrete structures prestressed with unbonded tendons. JGJ 92-2016. Beijing: MOHURD.

Mutsuyoshi, H., and A. Machida. 1993. "Behavior of prestressed concrete beams using FRP as external cable." *Spec. Publ.* 138: 401–418. https://doi.org/10.14359/3932.

Shahrooz, B. M., S. Boy, and T. M. Baseheart. 2002. "Flexural strengthening of four 76-year-old T-beams with various fiber-reinforced polymer systems: Testing and analysis." *ACI Struct. J.* 99 (5): 681–691. <a href="https://doi.org/10.14359/12308">https://doi.org/10.14359/12308</a>.

Sturm, A. B., P. Visintin, and D. J. Oehlers. 2021. "Design-oriented solutions for the shear capacity of reinforced concrete beams with and without fibers." *J. Struct. Eng.* 147 (6): 04021066. <a href="https://doi.org/10.1061/(ASCE)ST.1943-541X.0003023">https://doi.org/10.1061/(ASCE)ST.1943-541X.0003023</a>.

Sturm, A. B., P. Visintin, R. Seracino, G. W. Lucier, and D. J. Oehlers. 2020. "Flexural performance of pretensioned ultra-high performance fibre reinforced concrete beams with CFRP tendons." *Compos. Struct.* 243: 112223. https://doi.org/10.1016/j.compstruct.2020.112223.

Sun, Y., J.-H. Ji, H. Zhu, Z.-Q. Dong, P. Zhang, M. Yan, and C.-K. Soh. 2023. "Flexural behaviours of pretensioned prestressed concrete-UHDC composite beams reinforced with CFRP bars." *Compos. Struct.* 322: 117385. <a href="https://doi.org/10.1016/j.compstruct.2023.117385">https://doi.org/10.1016/j.compstruct.2023.117385</a>.

Tao, X., and G. Du. 1985. "Ultimate stress of unbonded tendons in partially prestressed concrete beams." *PCI J.* 30 (6): 72–91. https://doi.org/10.15554/pcij.11011985.72.91.

Terrasi, G. P. 2012. "Prefabricated thin-walled structural elements made from high performance concrete prestressed with CFRP wires." *J. Mater. Sci. Res.* 2 (1): 1–14. <a href="https://doi.org/10.5539/jmsr.v2n1p1">https://doi.org/10.5539/jmsr.v2n1p1</a>.

UHPC (Ultra-High Performance Concrete). 2022. *Technical standard for application of ultra-high performance concrete in bridge engineering*. DB/TJ 08-2401-2022. Shanghai, China: Local Standard of Shanghai.

Wang, H.-T., C. Tang, M.-S. Chen, J. Shi, and X.-Y. Cao. 2024. "Experimental study on the flexural performance of prestressed RC beams with post-tensioned CFRP strands." *Eng. Struct.* 309: 118118. <a href="https://doi.org/10.1016/j.engstruct.2024.118118">https://doi.org/10.1016/j.engstruct.2024.118118</a>.

Wang, X., J. Shi, G. Wu, L. Yang, and Z. Wu. 2015. "Effectiveness of basalt FRP tendons for strengthening of RC beams through the external prestressing technique." *Eng. Struct.* 101: 34–44. https://doi.org/10.1016/j.engstruct.2015.06.052.

Wu, T., Y. Sun, X. Liu, and Y. Cao. 2021. "Comparative study of the flexural behavior of steel fiber-reinforced lightweight aggregate concrete beams reinforced and prestressed with CFRP tendons." *Eng. Struct.* 233: 111901. <a href="https://doi.org/10.1016/j.engstruct.2021.111901">https://doi.org/10.1016/j.engstruct.2021.111901</a>.